

Detecting and Rectifying Noisy Labels: Similarity-based Methods

Huu-Tien Dang[†] Nguyen Duc-Thang^{*} Hoang Thanh-Tung[◊] Naoya Inoue^{†‡}

[†]JAIST ^{*}FPT Software AI Center [◊]Vietnam National University [‡]RIKEN

{s2310417, naoya-i}@jaist.ac.jp

Abstract

Label noise in datasets could damage the performance of neural net training. As the size of modern deep networks grows, there is a growing demand for automated tools for detecting such errors. In this paper, we propose model-agnostic error detection and rectification methods utilizing the penultimate feature from the trained neural network. Our idea is based on an observation that the similarity of penultimate features is higher for within-class data points than that of other class data points, making the probability of label occurrence within a tight-similar cluster, informative to detect and rectify errors. Extensive experiments show our method not only demonstrates high performances across various noises but also automatically rectifies these errors to improve the quality of datasets and model generalization.

1 Introduction

While the majority of knowledge in AI systems is learned through unsupervised learning, supervised learning is an indispensable step in building strong AI systems (c.f. the LeCun’s cake). For Large Language Models (LLMs) such as GPTs (Brown et al., 2020), LLaMA (Touvron et al., 2023a,b), and Gemini (Team et al., 2023), supervised learning accounts for only a small fraction of the total computation budget but has a significant impact on the models’ performance. Recent research (e.g. Zhou et al., 2023; Gunasekar et al., 2023) finds that high quality training data significantly improves performance while reducing the training cost by orders of magnitude. The need for automated tools for improving the quality of supervised learning data is rising as datasets and models are getting larger at an unprecedented speed.

Real world datasets contain a notable amount of errors (Beyer et al., 2020; Northcutt et al., 2021b). Previous works (Dau et al., 2022; Nguyen-Duc et al., 2023) showed that removing errors from the

training set improves the performance of AI models trained on that dataset. Automatic error rectification, however, is an underexplored topic. In this paper, we present a feature based approach for error detection and rectification in large scale datasets. We theoretically show that the similarity between the penultimate feature of a mislabeled data point and its true class data points is larger than that for data points from other classes (Sec. 3.1). Inspired by this observation, we develop simple yet effective similarity-based methods for detecting and rectifying label errors (Sec. 3.2). Extensive experiments demonstrate the superiorities of our methods across various settings (Sec. 4.2). Furthermore, our methods are *posthoc* and *model-agnostic* i.e. they can be applied to any deep neural network (DNN) architectures without the need for retraining.

2 Background and related work

Notation. Let $\mathbf{z} = (\mathbf{x}, \mathbf{y})$ be a data point, where $\mathbf{x} \in \mathcal{X}$ is an input and $\mathbf{y} \in \mathcal{Y}$ is an output. Let $\mathcal{D} = \{\mathbf{z}^{(i)}\}_{i=1}^n$ be a N -class noisy training dataset of n data points. Let $f : \mathcal{X} \mapsto \mathcal{Y}$ be a deep model parameterized by θ ; $\hat{\theta} = \arg \min_{\theta} \frac{1}{n} \sum_{i=1}^n \ell(\mathbf{z}^{(i)}, \theta)$ are optimal parameters of f measured on \mathcal{D} , where $\ell : \mathcal{Y} \times \mathcal{Y} \mapsto \mathbb{R}^+$ be the loss function. In this paper, $\mathbf{g}_{\hat{\theta}}(\mathbf{z}^{(i)}) = \nabla_{\theta} \ell(\mathbf{z}^{(i)}, \hat{\theta})$ is denoted as the gradient of the loss at $\hat{\theta}$ with respect to (w.r.t) θ .

Confident-based Error Detection Methods. Confident-based methods are based on the notion of *confident learning* (Northcutt et al., 2021a) that deriving label quality measurements by using predicted probability distribution (Wang and Mueller, 2022; Kuan and Mueller, 2022; Thyagarajan et al., 2022). Low confidence serves as a heuristic indicating the likelihood of a label noise. Given a data point \mathbf{z} with output label $\mathbf{y} = (y_1, \dots, y_k, \dots, y_N)$, the model’s predicted probabilities is $\mathbf{p} = (p_1, \dots, p_k, \dots, p_N)$ over N classes. Northcutt et al. (2021a) proposed three label quality

scoring methods:

(1) *Self-Confidence* (SC) refers to the estimated probability that the input \mathbf{x} belongs to the class associated with its given label k : $SC(\mathbf{z}, \mathbf{p}) = p_{y_k}$, for $k \in \{1, 2, \dots, N\}$.

(2) *Normalized-Margin* (NM) is the quantified difference between the model’s estimated probability of the given label and the probability of the most likely class: $NM(\mathbf{z}, \mathbf{p}) = p_{y_k} - p_{y^{*}}$, for $j^* = \arg \max_{j \neq k \in \{1, 2, \dots, N\}} p_{y_j}$

(3) *Confidence-Weighted Entropy* (CE) is the ratio of SC score and the normalized entropy: $CE(\mathbf{z}, \mathbf{p}) = \frac{p_{y_k}}{\mathcal{H}_N(\mathbf{p})}$, where $\mathcal{H}_N(\mathbf{p}) = -\frac{1}{\log N} \sum_{n=1}^N p_n \log(p_n)$.

Gradient-based Error Detection Methods.

Koh and Liang (2017) use Influence Function (IF)—a concept from robust statistic (Hampel, 1974)—for measuring the influence of a training data point to weights of a DNN. Dau et al. (2022) proposed a way to adapt IF and its variants i.e. *Gradient Dot Product* (GD; Charpiat et al. (2019a)), *Gradient Cosine* (GC; Charpiat et al. (2019a)), and *Tracing Gradient Decent* (TracIn; Pruthi et al. (2020)), for identifying erroneous in large-scale source code datasets. The idea is the gradients of error data points exhibit significantly large magnitudes and are opposite in direction to the gradients of normal data points. The algorithm computes the influence score of each data point in the noisy dataset with data points in a reference set. A more negative influence score means is more likely to be an error. Nguyen-Duc et al. (2023) use class information to improve the performance and stability of these gradient methods.

$$(1) IF(\mathbf{z}^{(i)}, \mathbf{z}^{(j)}) = -\frac{1}{n} \mathbf{g}_{\hat{\theta}}(\mathbf{z}^{(i)})^\top \mathcal{H}_{\hat{\theta}}^{-1} \mathbf{g}_{\hat{\theta}}(\mathbf{z}^{(j)}),$$

$$(2) GD(\mathbf{z}^{(i)}, \mathbf{z}^{(j)}) = \langle \mathbf{g}_{\hat{\theta}}(\mathbf{z}^{(i)}), \mathbf{g}_{\hat{\theta}}(\mathbf{z}^{(j)}) \rangle,$$

$$(3) GC(\mathbf{z}^{(i)}, \mathbf{z}^{(j)}) = \cos(\mathbf{g}_{\hat{\theta}}(\mathbf{z}^{(i)}), \mathbf{g}_{\hat{\theta}}(\mathbf{z}^{(j)})),$$

$$(4) TracIn(\mathbf{z}^{(i)}, \mathbf{z}^{(j)}) = \sum_{t=1}^T \eta_t GD(\mathbf{z}^{(i)}, \mathbf{z}^{(j)}),$$

where $\mathcal{H}_{\hat{\theta}}$ is the hessian matrix, T is the number of epochs, and η_t is the learning rate at epoch t .

Other Error Detection Methods. The rule-based approach (Chu et al., 2013) and statistics-based approach (Huang and He, 2018) are commonly used for structured data such as tabular data. Krishnan et al. (2016) combines active learning and convex models to detect errors on small classification datasets. These methods are not suitable for deep learning, as they assume convexity in the

model, and the rules in many large scale datasets are not easy to find and describe.

3 Method

3.1 Observation

We design experiments to randomly corrupt and inject noise into datasets. We then train a deep network using gradient descent on these altered datasets to measure how noisy data points behave on other data points. As an illustrative example in Fig. 1, we observed that the similarity between the mislabeled data points and their true class data point penultimate-layer representations is often higher than other class data points. We find that

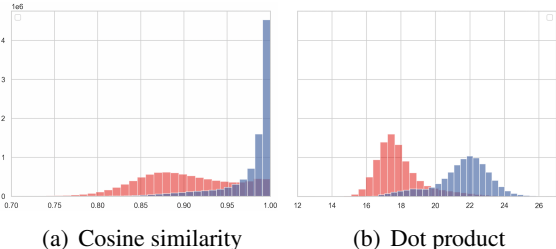


Figure 1: Distribution of (a) Cosine similarity and (b) Dot product over IMDB (Maas et al., 2011) with 10% noise. Blue bars represent the similarity between mislabeled data points and their true class data points, red bars represent the similarity between mislabeled data points and other class data points. Features are obtained from a trained BERT model.

this phenomenon persists across varying percentages of noises. To complement our observation, we provide a theoretical explanation in Appendix. B.

3.2 Algorithm

Our algorithm is detailed in Algorithm 1. It requires a small auxiliary dataset \mathcal{D}_{aux} , a similarity measure $\sigma(\cdot, \cdot)$. We denote $\phi^{(i)}$ and $\phi^{(j)}$ be the penultimate feature representations of $\mathbf{z}^{(i)}$ and $\mathbf{z}^{(j)}$ obtained from the trained model $f_{\hat{\theta}}$ respectively. We employ two primary similarity measures: Dot product ($DOT = \langle \phi^{(i)}, \phi^{(j)} \rangle$) and Cosine similarity ($COS = \frac{\langle \phi^{(i)}, \phi^{(j)} \rangle}{\|\phi^{(i)}\| \|\phi^{(j)}\|}$). We denote $\mathcal{S}(\mathcal{D}_{aux}, \mathbf{z}^{(i)})$ as k most similar to $\mathbf{z}^{(i)}$ in \mathcal{D}_{aux} .

Error Detection. Given a noisy dataset \mathcal{D} , for each data point $\mathbf{z}^{(i)} \in \mathcal{D}$ with label $y^{(i)}$, our algorithm finds $\mathcal{S}(\mathcal{D}_{aux}, \mathbf{z}^{(i)})$ such that every data point in \mathcal{D} but not in $\mathcal{S}(\mathcal{D}_{aux}, \mathbf{z}^{(i)})$ is at most similar to $\mathbf{z}^{(i)}$ as the least similar point in $\mathcal{S}(\mathcal{D}_{aux}, \mathbf{z}^{(i)})$ (line 6). We define a scoring function that return

Algorithm 1 Similarity-based Error Detection and Rectification

Require:

- 1: $\mathcal{D} = \{\mathbf{z}^{(i)}\}_{i=1}^n$: a noisy dataset
- 2: $\mathcal{D}_{\text{aux}} = \{\mathbf{z}^{(j)}\}_{j=1}^m$: an auxiliary dataset.
- 3: $\sigma(\cdot, \cdot)$: a similarity measure.
- 4: k : number of most similar data points.

Ensure: noisy data points in \mathcal{D} are rectified.

/* Error Detection */

- 5: **for** $\mathbf{z}^{(i)} \in \mathcal{D}$ **do**
 - 6: $\mathcal{S}(\mathcal{D}_{\text{aux}}, \mathbf{z}^{(i)}) = \{\mathbf{z}^{(j)} \in \mathcal{D}_{\text{aux}}$
 - s.t. $|\mathcal{S}(\mathcal{D}_{\text{aux}}, \mathbf{z}^{(i)})| = k$, and
 - $\sigma(\mathbf{z}^{(i)}, \mathbf{z}^{(j)}) \geq \max_{\mathbf{z}'^{(i)} \in \mathcal{D} \setminus \mathcal{S}(\mathcal{D}_{\text{aux}}, \mathbf{z}^{(i)})} \sigma(\mathbf{z}^{(i)}, \mathbf{z}'^{(i)})$
 - 7: $\mathbf{s}^{(i)} = \frac{1}{k} \sum_{\mathbf{z}^{(j)} \in \mathcal{S}(\mathcal{D}_{\text{aux}}, \mathbf{z}^{(i)})} \mathbb{I}(\mathbf{y}^{(j)} = \mathbf{y}^{(i)})$
 - 8: **end for**
 - 9: $\mathcal{D}^\uparrow = \text{sort}(\mathcal{D}, \text{key} = \mathbf{s}, \text{ascending} = \text{True})$
- /* Error Rectification */
- 10: **for** $\mathbf{z}^{(i)} \in \mathcal{D}_{:p}^\uparrow$ **do**
 - 11: $\mathbf{z}^{(i)} = (\mathbf{x}^{(i)}, \text{MODE}(\mathcal{S}(\mathcal{D}_{\text{aux}}, \mathbf{z}^{(i)})))$
 - 12: **return** \mathcal{D}
-

160
161
162
163
164
165
166
167
168
169
170
171
172
173
174
175
176
177
178
179
180
181
182
183
184

$\mathbf{s}^{(i)}$ —the probability of occurrence of label $\mathbf{y}^{(i)}$ in $\mathcal{S}(\mathcal{D}_{\text{aux}}, \mathbf{z}^{(i)})$ (line 7). The indicator $\mathbb{I}(\cdot)$ returns 1 if the condition holds. A lower \mathbf{s} is, more likely a label error. We sort the data points in \mathcal{D} in ascending order of \mathbf{s} and obtain the sorted \mathcal{D}^\uparrow (line 9).

Error Rectification. We select the first $p\%$ samples of ranked set \mathcal{D}^\uparrow denoted as $\mathcal{D}_{:p}^\uparrow$ and define a class decision rule $\text{MODE}(\cdot)$ that selects the label in $\mathcal{S}(\mathcal{D}_{\text{aux}}, \mathbf{z}^{(i)})$ has the highest probability and greater than threshold τ . Otherwise, the label of $\mathbf{z}^{(i)}$ remains unchanged (line 11).

4 Experiment

4.1 Experiment Setting

Dataset and Model. We evaluate our method on two common benchmarks: Sentiment Analysis on IMDB (Maas et al., 2011) and Short Text Classification on Snippets (Phan et al., 2008). We use BERT (Devlin et al., 2019) as the standard model for all settings.

Modeling Realistic Noise. We construct three realistic, human-originated types of noise: (1) *Uniform noise*: we randomly select data points and change the label to a different class. (2) *Systematic ambiguity noise*: we establish a rule h , which maps data points in a specific class to another fixed one.

This means that the labels of selected instances in class i are flipped to $h(i)$. To ensure distinctiveness, the mapping function h adheres to the condition $h(i) \neq h(j) \forall i, j = \{1, \dots, N\}$, and $i \neq j$. This noise models the situations where inputs from multiple annotators are often aggregated, the resulting differences in annotations can serve as a model of systematic noise derived from human disagreements. (3) *Concentrated noise*: we select data points that are densely clustered and change their labels to target labels. We simulate scenarios where the datasets are poisoned by malicious to evaluate the sanitization ability of methods against data poisoning attacks.

Setting. For each dataset, we construct groups of various sizes of noisy samples by corrupting the label of $p\%$ of the original training data. We construct the auxiliary dataset \mathcal{D}_{aux} by randomly selecting m samples from the validation set. We fine-tune BERT on noisy dataset \mathcal{D} and select the best checkpoint measure on the validation set. We select top $t\%$ ranked samples in $\mathcal{D}_{:p}^\uparrow$ and use error detection accuracy for evaluation. After rectifying/removing ranked samples (potentially noisy samples), we re-train the model and report the test accuracy and error reduction rate. Details of the dataset, model, and implementations are in Appendix A.

4.2 Main Result and Analysis

Error detection accuracy. (1) Fig. 2 shows the error detection accuracy of methods with three types of noise with different percentages. As a result, when t increases the performance of gradient-based methods *drastically decreases*. This pattern is observed in all three types of noise across different percentages and in both Snippets (Fig. 4) and IMDB (Fig. 5). This result shows that the gradient-based methods are unstable and less inconsistent. (2) Confident-based methods are precise with uniform noises and systematic ambiguity noise yet struggle with concentrated noise (Fig. 2c). (3) Sim-Cos and Sim-Dot have high detection accuracy and slightly decrease when t increases with difference noise. This confirmed that the Similarity-based methods are effective and more robust to ambiguity and concentrated noises than gradient-/confident-based methods. (4) We observe that Sim-Dot often has low detection accuracy on IMDB (Fig. 5). We theoretically proved that for classification datasets with N classes, the similarity of within-class data

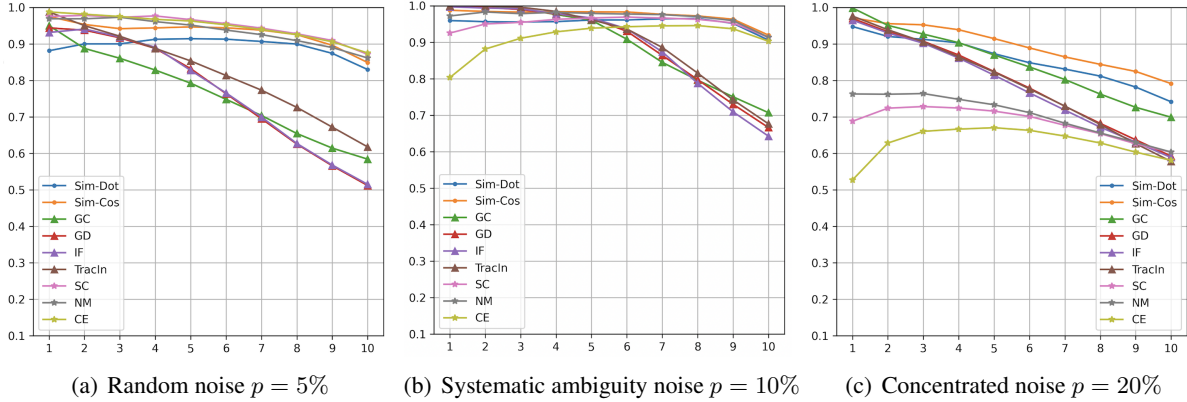


Figure 2: Error detection accuracy of methods measure on Snippets. The x-axis in the figures presents the change of t from 10 → 100%.

Table 1: Test accuracy after remove/rectify potential noise samples on Snippets with 20% noise. The **best** and runner-up are marked.

Method	Random noise		Ambiguity noise		Concentrated noise	
	Removed	Rectified	Removed	Rectified	Removed	Rectified
Acc. (under noise)	88.64 (+0.00)	—	82.50 (+0.00)	—	79.38 (+0.00)	—
Confident-W. Entropy	83.02 (-5.62)	—	84.38 (+1.88)	—	77.50 (-1.88)	—
Normalize-Margin	87.19 (-1.45)	—	87.01 (+4.51)	—	77.89 (-1.49)	—
Self-Confidence	86.05 (-2.59)	—	87.36 (+4.86)	—	78.02 (-1.36)	—
Influence Function	83.24 (-5.40)	—	81.71 (-0.79)	—	79.51 (+0.13)	—
Gradient-Cosine	73.81 (-14.83)	—	83.33 (+0.83)	—	82.23 (+2.85)	—
Gradient-Dot	86.53 (-2.11)	—	82.01 (-0.49)	—	78.68 (-0.70)	—
TracIn	85.48 (-3.16)	—	81.71 (-0.79)	—	76.67 (-2.71)	—
Sim-Cos	89.43 (+0.79)	87.85 (-0.79)	85.00 (+2.50)	83.73 (+1.23)	<u>81.53</u> (+2.15)	83.38 (+4.00)
Sim-Dot	86.71 (-1.93)	87.32 (-1.32)	82.98 (+0.48)	83.95 (+1.45)	<u>81.53</u> (+2.15)	<u>81.97</u> (+2.59)

points is approximately $N - 1$ times larger than other class data points. For IMDB where $N = 2$, this fraction becomes approximately 1. That explains why Sim-Dot does not work well on IMDB. Mathematical details are in Appendix. B. (5) Sim-Cos, consistently outperforms Sim-Dot by a large margin for all settings. We explain from the standpoint of *feature normalization*. By definition, Cosine similarity can be seen as the normalized Dot product. In Fig. 4 (b), we empirically show that the noisy samples have L_2 -norm smaller than normal samples. Therefore, when dividing the feature of data points by its norm, the similarity between noisy and normal data points tends to be larger, leading to a more distinct distribution of similarities.

Improving datasets and model generalization. Tab.1 shows a significant improvement in the test accuracy when removing/rectifying concentrated noise and systematic ambiguity noise. Nevertheless, a counter-intuitive observation regarding ran-

dom noise shows that removing/rectifying noise reduces the generalization of models, even when detection accuracy is high. We posit that deep models are robust to massive random noise (Rolnick et al., 2017), then as the training process, the model also memorizes the noise, approaches the optimum, and the gradient of noise becomes smaller. The effect of noise, therefore, also decreases as the model converges. When removing noise, the model degrades the feature representation of noise samples and loses the generalization to unseen samples.

5 Conclusion

We introduce similarity-based algorithms for detecting and rectifying errors on large-scale datasets. We theoretically show that the similarity between the penultimate feature’s data points is useful for detecting errors. Experiment results demonstrated the superior performance of our methods, and their capability to improve datasets quality and model generalization.

276 Limitations

277 We discuss the limitations of similarity-based methods:
278 (1) The optimal detection accuracy of Sim-
279 Cos and Sim-Dot unfortunately based on empirical
280 validation, and depends on the choice of k and \mathcal{D}_{aux}
281 and also with different datasets and model architec-
282 tures. (2) The generalization of models under the
283 removal or rectification of noise remains uncertain,
284 due to the limited exploration of datasets.

285 Ethics Statement

286 We consider only the public datasets and create
287 artificial noises for evaluation. We do not pose any
288 concern about the quality of the original datasets.

289 Acknowledgements

290 We thank Thu Tran and the anonymous reviewers
291 for their constructive feedback.

292 References

- 293 Naman Agarwal, Brian Bullins, and Elad Hazan. 2017.
294 Second-order stochastic optimization for machine
295 learning in linear time. *The Journal of Machine
296 Learning Research*, 18(1):4148–4187.
- 297 Lucas Beyer, Olivier J. Hénaff, Alexander Kolesnikov,
298 Xiaohua Zhai, and Aäron van den Oord. 2020. [Are
299 we done with imagenet?](#) *CoRR*, abs/2006.07159.
- 300 Tom Brown, Benjamin Mann, Nick Ryder, Melanie
301 Subbiah, Jared D Kaplan, Prafulla Dhariwal, Arvind
302 Neelakantan, Pranav Shyam, Girish Sastry, Amanda
303 Askell, et al. 2020. Language models are few-shot
304 learners. *Advances in neural information processing
305 systems*, 33:1877–1901.
- 306 Guillaume Charpiat, Nicolas Girard, Loris Felardos,
307 and Yuliya Tarabalka. 2019a. Input similarity from
308 the neural network perspective. *Advances in Neural
309 Information Processing Systems*, 32.
- 310 Guillaume Charpiat, Nicolas Girard, Loris Felardos,
311 and Yuliya Tarabalka. 2019b. Input similarity from
312 the neural network perspective. *Advances in Neural
313 Information Processing Systems*, 32.
- 314 Xu Chu, Ihab F. Ilyas, and Paolo Papotti. 2013. [Holistic
315 data cleaning: Putting violations into context.](#) In
316 *2013 IEEE 29th International Conference on Data
317 Engineering (ICDE)*, pages 458–469.
- 318 Anh TV Dau, Nghi DQ Bui, Thang Nguyen-Duc, and
319 Hoang Thanh-Tung. 2022. Towards using data-
320 influence methods to detect noisy samples in source
321 code corpora. In *37th IEEE/ACM International Con-
322 ference on Automated Software Engineering*, pages
323 1–3.

- 324 Jacob Devlin, Ming-Wei Chang, Kenton Lee, and
325 Kristina Toutanova. 2019. [BERT: Pre-training of
326 deep bidirectional transformers for language under-
327 standing.](#) In *Proceedings of the 2019 Conference of
328 the North American Chapter of the Association for
329 Computational Linguistics: Human Language Tech-
330 nologies, Volume 1 (Long and Short Papers)*, pages
331 4171–4186, Minneapolis, Minnesota. Association for
332 Computational Linguistics.
- 333 Suriya Gunasekar, Yi Zhang, Jyoti Aneja, Caio
334 César Teodoro Mendes, Allie Del Giorno, Sivakanth
335 Gopi, Mojgan Javaheripi, Piero Kauffmann, Gustavo
336 de Rosa, Olli Saarikivi, et al. 2023. Textbooks are all
337 you need. *arXiv preprint arXiv:2306.11644*.
- 338 Frank R. Hampel. 1974. [The influence curve and its
339 role in robust estimation.](#) *Journal of the American
340 Statistical Association*, 69(346):383–393.
- 341 Kazuaki Hanawa, Sho Yokoi, Satoshi Hara, and Ken-
342 taro Inui. 2021. [Evaluation of similarity-based ex-
343 planations.](#) In *International Conference on Learning
344 Representations*.
- 345 Zhipeng Huang and Yeye He. 2018. Auto-detect: Data-
346 driven error detection in tables. In *Proceedings of
347 the 2018 International Conference on Management
348 of Data*, pages 1377–1392.
- 349 Pang Wei Koh and Percy Liang. 2017. Understanding
350 black-box predictions via influence functions. In
351 *International conference on machine learning*, pages
352 1885–1894. PMLR.
- 353 Sanjay Krishnan, Jiannan Wang, Eugene Wu, Michael J.
354 Franklin, and Ken Goldberg. 2016. [Activeclean: Inter-
355 active data cleaning for statistical modeling.](#) *Proc.
356 VLDB Endow.*, 9(12):948–959.
- 357 Johnson Kuan and Jonas Mueller. 2022. Model-agnostic
358 label quality scoring to detect real-world label errors.
359 In *ICML DataPerf Workshop*.
- 360 Ilya Loshchilov and Frank Hutter. 2019. [Decoupled
361 weight decay regularization.](#) In *International Confer-
362 ence on Learning Representations*.
- 363 Andrew L. Maas, Raymond E. Daly, Peter T. Pham,
364 Dan Huang, Andrew Y. Ng, and Christopher Potts.
365 2011. [Learning word vectors for sentiment analysis.](#)
366 In *Proceedings of the 49th Annual Meeting of the
367 Association for Computational Linguistics: Human
368 Language Technologies*, pages 142–150, Portland,
369 Oregon, USA. Association for Computational Lin-
370 guistics.
- 371 Thang Nguyen-Duc, Hoang Thanh-Tung, Quan Hung
372 Tran, Dang Huu-Tien, Hieu Nguyen, Anh T. V. Dau,
373 and Nghi Bui. 2023. [Class based influence functions
374 for error detection.](#) In *Proceedings of the 61st Annual
375 Meeting of the Association for Computational Lin-
376 guistics (Volume 2: Short Papers)*, pages 1204–1218,
377 Toronto, Canada. Association for Computational Lin-
378 guistics.

379	Curtis Northcutt, Lu Jiang, and Isaac Chuang. 2021a.	Wei-Chen Wang and Jonas Mueller. 2022. Detecting la-	435
380	Confident learning: Estimating uncertainty in dataset	bel errors in token classification data. <i>arXiv preprint</i>	436
381	labels. <i>Journal of Artificial Intelligence Research</i> ,	<i>arXiv:2210.03920</i> .	437
382	70:1373–1411.		
383	Curtis G Northcutt, Anish Athalye, and Jonas Mueller.	Chunting Zhou, Pengfei Liu, Puxin Xu, Srinivas Iyer, Jiao	438
384	2021b. Pervasive label errors in test sets destabilize	Sun, Yuning Mao, Xuezhe Ma, Avia Efrat, Ping Yu,	439
385	machine learning benchmarks.	Lili Yu, et al. 2023. Lima: Less is more for alignment.	440
386	In <i>Thirty-fifth Conference on Neural Information Processing Systems</i>	<i>arXiv preprint arXiv:2305.11206</i> .	441
387	<i>Datasets and Benchmarks Track (Round 1)</i> .		
388	Pouya Pezeshkpour, Sarthak Jain, Byron Wallace, and	A Implementation detail	442
389	Sameer Singh. 2021. An empirical comparison of in-	A.1 Dataset and Model	443
390	stance attribution methods for NLP. In <i>Proceedings</i>	Snippets (Phan et al., 2008) is an open dataset	444
391	of the 2021 Conference of the North American Chapter	of web search snippets retrieved from Google	445
392	of the Association for Computational Linguistics:	Search with 8 domains including Business, Com-	446
393	<i>Human Language Technologies</i> , pages 967–975, On-	puters, Culture-Arts-Entertainment, Education-	447
394	line. Association for Computational Linguistics.	Science, Engineering, Health, Politics-Society,	448
395	Xuan-Hieu Phan, Le-Minh Nguyen, and Susumu	and Sports. The training data and testing	449
396	Horiguchi. 2008. Learning to classify short and	data include 10,060 and 2,280 snippets respec-	450
397	sparse text & web with hidden topics from large-	tively. For validation purposes, we randomly	451
398	scale data collections. In <i>Proceedings of the 17th</i>	split original training data into train/valid with	452
399	<i>international conference on World Wide Web</i> , pages	the ratio of 8048/2012. The dataset can be	453
400	91–100.	found at http://jwebpro.sourceforge.net/data-web-snippets.tar.gz .	454
401	Garima Pruthi, Frederick Liu, Satyen Kale, and Mukund	IMDB (Maas et al., 2011) is the most com-	455
402	Sundararajan. 2020. Estimating training data influ-	mon benchmark for Sentiment Analysis task.	456
403	ence by tracing gradient descent. <i>Advances in Neural</i>	IMDB includes 50000 reviews from the Inter-	457
404	<i>Information Processing Systems</i> , 33:19920–19930.	net Movie Database website with original 25000	458
405	David Rolnick, Andreas Veit, Serge Belongie, and Nir	negative and 25000 positive reviews. For val-	459
406	Shavit. 2017. Deep learning is robust to massive	idation purposes, we randomly split into train-	460
407	label noise. <i>arXiv preprint arXiv:1705.10694</i> .	ing, validation, and test sets of sizes 15000,	461
408	Nitish Srivastava, Geoffrey Hinton, Alex Krizhevsky,	5000, and 25000. The IMDB dataset can	462
409	Ilya Sutskever, and Ruslan Salakhutdinov. 2014.	be found at https://ai.stanford.edu/~amaas/data/sentiment/	463
410	Dropout: A simple way to prevent neural networks		464
411	from overfitting.		465
412	<i>Journal of Machine Learning Research</i> , 15(56):1929–1958.		
413	Gemini Team, Rohan Anil, Sebastian Borgeaud,	BERT (Devlin et al., 2019) stands for Bidirec-	466
414	Yonghui Wu, Jean-Baptiste Alayrac, Jiahui Yu,	tional Encoder Representations from Transformers.	467
415	Radu Soricut, Johan Schalkwyk, Andrew M Dai,	BERT is one of the most standard used pre-trained	468
416	Anja Hauth, et al. 2023. Gemini: a family of	model for language understanding tasks. In all	469
417	highly capable multimodal models. <i>arXiv preprint</i>	settings, we use BERT base uncased version.	470
418	<i>arXiv:2312.11805</i> .		
419	Aditya Thyagarajan, Elías Snorrason, Curtis Northcutt,	A.2 Experiment detail	471
420	and Jonas Mueller. 2022. Identifying incorrect an-	BERT was trained with AdamW (Loshchilov and	472
421	notations in multi-label classification data. <i>arXiv</i>	Hutter, 2019) with learning rate $\eta = 5e - 5$,	473
422	<i>preprint arXiv:2211.13895</i> .	momentum $\beta = (0.9, 0.999)$, cross entropy loss,	474
423	Hugo Touvron, Thibaut Lavril, Gautier Izacard, Xavier	batch-size of 16 with 15 epochs. For regularization,	475
424	Martinet, Marie-Anne Lachaux, Timothée Lacroix,	we use Dropout (Srivastava et al., 2014) of	476
425	Baptiste Rozière, Naman Goyal, Eric Hambro, Faisal	0.2. We choose $p = \{5\%, 10\%, 20\%\}$, $m =$	477
426	Azhar, et al. 2023a. Llama: Open and effi-	1000, $k = \{1, 2, 5, 10, 20, 50, 100, 200\}$, $t =$	478
427	cient foundation language models. <i>arXiv preprint</i>	$\{10\%, 20\%, \dots, 100\%\}$, and $\tau = 0.8$. We compute	479
428	<i>arXiv:2302.13971</i> .	the IF score for BERT with the last layer gradient as	480
429	Hugo Touvron, Louis Martin, Kevin Stone, Peter Al-	previous works (Pezeshkpour et al., 2021; Hanawa	481
430	bert, Amjad Almahairi, Yasmine Babaee, Nikolay	et al., 2021) and use LiSSA (Agarwal et al., 2017)	482
431	Bashlykov, Soumya Batra, Prajjwal Bhargava, Shruti	to approximate the Hessian. For TracIn method, we	483
432	Bhosale, et al. 2023b. Llama 2: Open founda-		
433	tion and fine-tuned chat models. <i>arXiv preprint</i>		
434	<i>arXiv:2307.09288</i> .		

484 calculate the influence score from the first epoch
 485 to the best epoch. We run experiments on 4 seeds
 486 = {16, 32, 64, 128} and aggregate the results by
 487 taking the mean of these 4 seeds. A Nvidia RTX
 488 GeForce 3090 Ti was used to run experiments. Our
 489 implementation was attached to the supplementary
 490 materials.

491 B Theoretical Analysis

492 We consider a deep network received input $\mathbf{x} \in \mathbb{R}^d$,
 493 where d is the input dimension. Let δ be the soft-
 494 max activation function, $\mathbf{b} \in \mathbb{R}^N$ be the bias.
 495 Given an output function ϕ_W parameterized by
 496 $W \in \mathbb{R}^{N \times d}$. For two inputs $\mathbf{x}^{(i)}$ and $\mathbf{x}^{(j)}$ we have
 497 two output vectors $\phi_W(\mathbf{x}^{(i)})$ and $\phi_W(\mathbf{x}^{(j)})$ respec-
 498 tively. As seen by a deep network, we can mea-
 499 sure the influence between $\mathbf{x}^{(i)}$ and $\mathbf{x}^{(j)}$ by quan-
 500 tifying how much $\phi_W(\mathbf{x}^{(i)})$ change would change
 501 $\phi_W(\mathbf{x}^{(j)})$ as well. If $\mathbf{x}^{(i)}$ and $\mathbf{x}^{(j)}$ have high sim-
 502 ilarity, then $\mathbf{x}^{(i)}$ have high influence on $\mathbf{x}^{(j)}$ and
 503 changing $\phi_W(\mathbf{x}^{(i)})$ have large effect on $\phi_W(\mathbf{x}^{(j)})$.
 504 Otherwise, if they have low similarity, then $\mathbf{x}^{(i)}$
 505 have low influence on $\mathbf{x}^{(j)}$ and changing $\phi_W(\mathbf{x}^{(i)})$
 506 have small effect on $\phi_W(\mathbf{x}^{(j)})$. To measure the
 507 similarity between data points, we employ a sym-
 508 metric kernel proposed by Charpiat et al. (2019b):
 509 The Inner Product

$$510 \mathcal{K}(\mathbf{x}^{(i)}, \mathbf{x}^{(j)}) = \left\langle \nabla_W \phi_W(\mathbf{x}^{(i)}), \nabla_W \phi_W(\mathbf{x}^{(j)}) \right\rangle, \quad (1)$$

511 We choice ϕ is the Cross Entropy between softmax
 512 activation output $\hat{\mathbf{y}} = \delta(W\mathbf{x} + \mathbf{b})$ and true dis-
 513 tribution \mathbf{y} . We have $\phi_W(\mathbf{x}) = \ell(\hat{\mathbf{y}}, \mathbf{y}; W)$. For
 514 simplicity, we remove the bias term. Let denote
 515 $\mathbf{u} = W\mathbf{x}$ and $\ell(\hat{\mathbf{y}}, \mathbf{y}) = \ell(\hat{\mathbf{y}}, \mathbf{y}; W)$. Using the
 516 chain rule:

$$517 \nabla_W \ell(\hat{\mathbf{y}}, \mathbf{y}) = \text{vec} \left(\frac{\partial \ell(\hat{\mathbf{y}}, \mathbf{y})}{\partial W} \right) \\ 518 = \text{vec} \left(\frac{\partial \ell(\hat{\mathbf{y}}, \mathbf{y})}{\partial \mathbf{u}} \frac{\partial \mathbf{u}}{\partial W} \right) \\ 519 = \nabla_{\mathbf{u}} \ell(\hat{\mathbf{y}}, \mathbf{y}) \mathbf{x}^\top, \quad (2)$$

520 where $\text{vec} \left(\frac{\partial \ell(\hat{\mathbf{y}}, \mathbf{y})}{\partial W} \right)$ is the vectorization of the
 521 derivative of the loss ℓ with respect to W . The
 522 partial $\frac{\partial \ell(\hat{\mathbf{y}}, \mathbf{y})}{\partial \mathbf{u}}$ is

$$523 \frac{\partial \ell(\hat{\mathbf{y}}, \mathbf{y})}{\partial \mathbf{u}} = \frac{\partial \ell(\hat{\mathbf{y}}, \mathbf{y})}{\partial \hat{\mathbf{y}}} \frac{\partial \hat{\mathbf{y}}}{\partial \mathbf{u}} \quad (3)$$

524 The first term on the right hand side of Eqn. 3 is
 525 partial derivatives of the loss w.r.t the predicted

526 output $\hat{\mathbf{y}}$. Regarding to the fact: \mathbf{y} is the one-hot
 527 vector present label k has element $y_k = 1$ and
 528 $y_i = 0$ if $i \neq k$. We have:

$$\begin{aligned} \frac{\partial \ell(\hat{\mathbf{y}}, \mathbf{y})}{\partial \hat{\mathbf{y}}} &= \left[\frac{\partial \ell(\hat{\mathbf{y}}, \mathbf{y})}{\partial \hat{y}_1} \dots \frac{\partial \ell(\hat{\mathbf{y}}, \mathbf{y})}{\partial \hat{y}_k} \dots \frac{\partial \ell(\hat{\mathbf{y}}, \mathbf{y})}{\partial \hat{y}_N} \right] \\ &= \left[0 \dots \frac{1}{y_k} \dots 0 \right] \end{aligned} \quad (4)$$

529 The second term is the matrix comprises partial
 530 derivatives of the predicted output $\hat{\mathbf{y}}$ w.r.t \mathbf{u} . Re-
 531 garding to the fact:
 532

$$\frac{\partial \hat{\mathbf{y}}}{\partial \mathbf{u}} = \begin{bmatrix} \frac{\partial \hat{y}_1}{\partial u_1} & \frac{\partial \hat{y}_1}{\partial u_2} & \dots & \frac{\partial \hat{y}_1}{\partial u_N} \\ \vdots & \vdots & \ddots & \vdots \\ \frac{\partial \hat{y}_k}{\partial u_1} & \frac{\partial \hat{y}_k}{\partial u_2} & \dots & \frac{\partial \hat{y}_k}{\partial u_N} \\ \vdots & \vdots & \ddots & \vdots \\ \frac{\partial \hat{y}_N}{\partial u_1} & \frac{\partial \hat{y}_N}{\partial u_2} & \dots & \frac{\partial \hat{y}_N}{\partial u_N} \end{bmatrix} \quad (5)$$

533 Substitute Eqn. 5 and Eqn. 4 into Eqn. 3, we get

$$\begin{aligned} \frac{\partial \ell(\hat{\mathbf{y}}, \mathbf{y})}{\partial \mathbf{u}} &= \\ &\left[\frac{\partial \ell(\hat{\mathbf{y}}, \mathbf{y})}{\partial \hat{y}_k} \frac{\partial \hat{y}_k}{\partial u_1} \dots \frac{\partial \ell(\hat{\mathbf{y}}, \mathbf{y})}{\partial \hat{y}_k} \frac{\partial \hat{y}_k}{\partial u_k} \dots \frac{\partial \ell(\hat{\mathbf{y}}, \mathbf{y})}{\partial \hat{y}_k} \frac{\partial \hat{y}_k}{\partial u_N} \right] \end{aligned} \quad (6)$$

538 Given a softmax activation function δ for class
 539 k : Case 1: $i = k$, we compute the derivative of
 540 softmax output \hat{y}_k w.r.t u_k :

$$\begin{aligned} \frac{\partial \hat{y}_k}{\partial u_k} &= \frac{\partial}{\partial u_k} \left(\frac{e^{u_k}}{\sum_{i=1}^N e^{u_i}} \right) \\ &= \frac{e^{u_k} \left(\sum_{i=1}^N e^{u_i} \right) - e^{u_k} \cdot e^{u_k}}{\left(\sum_{i=1}^N e^{u_i} \right)^2} \\ &= \hat{y}_k (1 - \hat{y}_k) \end{aligned} \quad (7)$$

541 Case 2: $i \neq k$, we compute the derivative of soft-
 542 max output \hat{y}_k w.r.t u_i :

$$\frac{\partial \hat{y}_k}{\partial u_i} = \frac{\partial}{\partial u_i} \left(\frac{e^{u_k}}{\sum_{i=1}^N e^{u_i}} \right) \quad (8)$$

543 Using the chain rule, we get:

$$\frac{\partial \hat{y}_k}{\partial u_i} = - \frac{e^{u_k} \cdot e^{u_i}}{\left(\sum_{i=1}^N e^{u_i} \right)^2} = -\hat{y}_k \hat{y}_i \quad (9)$$

544 Substitute Eqn. 7 and Eqn. 9 into Eqn. 6, we get a
 545 column vector:

$$\nabla_{\mathbf{u}} \ell(\hat{\mathbf{y}}, \mathbf{y}) = [-\hat{y}_1 \dots 1 - \hat{y}_k \dots -\hat{y}_N]^\top \quad (10)$$

552 The inner product kernel in Eqn. 2 become:

$$553 \quad \mathcal{K}(\mathbf{x}^{(i)}, \mathbf{x}^{(j)}) = \overbrace{\nabla_{\mathbf{u}} \ell(\hat{\mathbf{y}}^{(i)}, \mathbf{y}^{(i)})^\top \nabla_{\mathbf{u}} \ell(\hat{\mathbf{y}}^{(j)}, \mathbf{y}^{(j)})}^{\mathbf{G}^{(ij)}} \\ 554 \quad \cdot (\mathbf{x}^{(j)\top} \mathbf{x}^{(i)}) \quad (11)$$

555 We denote $\mathbf{G}^{(ij)}$ as the dot product of two gradients
556 of the loss at $\mathbf{x}^{(i)}$ and $\mathbf{x}^{(j)}$. Suppose input $\mathbf{x}^{(i)}$ and
557 input $\mathbf{x}^{(j)}$ have label k and k' corresponding. We
558 have

$$559 \quad \mathbf{G}^{(ij)} = \left[-\hat{y}_1^{(i)} \cdots 1 - \hat{y}_k^{(i)} \cdots - \hat{y}_N^{(i)} \right] \begin{bmatrix} -\hat{y}_1^{(j)} \\ \vdots \\ 1 - \hat{y}_{k'}^{(j)} \\ \vdots \\ -\hat{y}_N^{(j)} \end{bmatrix} \quad (12)$$

560 we consider 2 cases:

561 If $k = k'$:

$$562 \quad \mathbf{G}_{k=k'}^{(ij)} = \hat{y}_1^{(i)} \hat{y}_1^{(j)} + \cdots + (1 - \hat{y}_k^{(i)})(1 - \hat{y}_k^{(j)}) \\ 563 \quad + \cdots + \hat{y}_N^{(i)} \hat{y}_N^{(j)} \\ 564 \quad = (1 - \hat{y}_k^{(i)})(1 - \hat{y}_k^{(j)}) + \sum_{n=1, n \neq k}^N \hat{y}_n^{(i)} \hat{y}_n^{(j)} \quad (13)$$

565 If $k \neq k'$:

$$566 \quad \mathbf{G}_{k \neq k'}^{(ij)} = \hat{y}_1^{(i)} \hat{y}_1^{(j)} + \cdots + (1 - \hat{y}_k^{(i)})(-\hat{y}_k^{(j)}) + \\ 567 \quad (1 - \hat{y}_{k'}^{(j)})(-\hat{y}_{k'}^{(i)}) + \cdots + \hat{y}_N^{(i)} \hat{y}_N^{(j)} \\ 568 \quad = \hat{y}_k^{(j)}(\hat{y}_k^{(i)} - 1) + \hat{y}_{k'}^{(i)}(\hat{y}_{k'}^{(j)} - 1) \\ 569 \quad + \sum_{n=1, n \neq k, n \neq k'}^N \hat{y}_n^{(i)} \hat{y}_n^{(j)} \quad (14)$$

570 During the training process, the model is more
571 confident about the labels of data points, indicating
572 the value of $\hat{y}_k^{(i)}$ and $\hat{y}_{k'}^{(j)}$ being closer to 1. Assume
573 a well-trained model, and $\hat{y}_k^{(i)} \approx \hat{y}_{k'}^{(j)} = \alpha$; $\hat{y}_n^{(i)} =$
574 $\hat{y}_n^{(j)} \approx \epsilon = \frac{1-\alpha}{N-1}$. ($n \neq k$ and $n \neq k'$). Substitute
575 these values into Eqn. 13 and Eqn. 14, we get :

$$576 \quad \mathbf{G}_{k=k'}^{(ij)} \approx (1 - \alpha)^2 + \epsilon^2(N - 1) \quad (15)$$

$$577 \quad \mathbf{G}_{k \neq k'}^{(ij)} \approx -\frac{N(1 - \alpha)^2}{(N - 1)^2} = -\epsilon^2 N \quad (16)$$

578 As N become very large with deep learning dataset
579 and ϵ small, the magnitude of $\mathbf{G}_{k \neq k'}^{(ij)}$ is close to

580 0 for $k \neq k'$. That means data points in different
581 classes tend to be pushed into different orthogonal
582 sub-spaces. Let's consider the the magnitude of
583 $\mathbf{G}_{k=k'}^{(ij)}$ and $\mathbf{G}_{k \neq k'}^{(ij)}$, divide $|\mathbf{G}_{k=k'}^{(ij)}|$ by $|\mathbf{G}_{k \neq k'}^{(ij)}|$, we
584 get:

$$585 \quad \frac{\mathcal{K}_{k=k'}^{(ij)}}{\mathcal{K}_{k \neq k'}^{(ij)}} = \frac{|\mathbf{G}_{k=k'}^{(ij)}|}{|\mathbf{G}_{k \neq k'}^{(ij)}|} \approx \frac{|(1 - \alpha)^2 + \epsilon^2(N - 1)|}{|- \epsilon^2 N|} \\ 586 \quad \approx \frac{\epsilon^2(N - 1)^2 + \epsilon^2(N - 1)}{\epsilon^2 N} \approx N - 1 \quad (17)$$

587 Here, the kernel $\mathcal{K}_{k=k'}^{(ij)}$ ($\mathcal{K}_{k \neq k'}^{(ij)}$) represents the sim-
588 ilarity between $\mathbf{x}^{(i)}$ and $\mathbf{x}^{(j)}$ when they share the
589 same label (different labels). This explains why
590 mislabeled data points are often more similar to
591 true class data points than data points in other
592 classes.

593 **Similarity-based methods do not work well on**
594 **IMDB (Fig. 5).** For the IMDB dataset with $N =$
595 2, the fraction are approximately 1. Hence, the
596 similarity between data points within the same class
597 and those in the remaining class does not have a
598 significant gap.

C Ablation studies

C.1 The effect of the size of \mathcal{D}_{aux} , the number of k , and τ .

599 **The effect of the size of \mathcal{D}_{aux} .** We change the
600 size of \mathcal{D}_{aux} from 100 to 1500, fix $k = 100$. Tab. 2
601 and Tab. 3 show the change in error detection accu-
602 racy as the size of \mathcal{D}_{aux} changes. We observed that:
603 (1) the detection accuracy of the methods increases
604 as the size of \mathcal{D}_{aux} increases. This is true for both
605 Snippets and IMDB, Sim-Cos and Sim-Dot, and
606 for all levels of noise {5%, 10%, 20%}. (2) The
607 accuracy gains are larger for smaller \mathcal{D}_{aux} values. (3)
608 Sim-Cos outperforms Sim-Dot for all noise levels
609 and most \mathcal{D}_{aux} values.

610 **The effect of k .** Tab. 4 and Tab. 5 show that Sim-
611 Cos and Sim-Dot have accuracy increase as k in-
612 creases for all noise levels {5%, 10%, 20%} and
613 for most values of k . The accuracy gains are often
614 larger for smaller values of k . Sim-Cos outper-
615 forms Sim-Dot, especially for larger values of k for
616 all noise levels and most values of k . The impact of
617 noise on detection accuracy with Snippets is gen-
618 erally small, but it increases with k . For Sim-Cos
619 with 20% noise in Tab. 4, the accuracy starts to
620 621 622 623

Table 2: The effect of the size of \mathcal{D}_{aux} , setting with Snippets.

Method	5% noise	10% noise	20% noise
Sim-Cos@100	16.91	22.63	31.69
Sim-Cos@200	51.99	40.67	65.25
Sim-Cos@300	57.46	56.96	80.23
Sim-Cos@400	60.45	72.38	86.45
Sim-Cos@500	75.37	78.60	86.88
Sim-Cos@600	77.36	78.60	89.93
Sim-Cos@700	82.58	78.48	93.10
Sim-Cos@800	85.07	78.60	92.91
Sim-Cos@900	86.07	79.72	93.16
Sim-Cos@1000	86.56	80.01	93.28
Sim-Cos@1500	88.06	80.97	94.28
Sim-Dot@100	16.91	22.63	31.69
Sim-Dot@200	51.74	40.92	64.26
Sim-Dot@300	57.96	56.59	79.42
Sim-Dot@400	61.19	70.64	86.82
Sim-Dot@500	74.62	78.23	87.01
Sim-Dot@600	76.36	78.10	88.87
Sim-Dot@700	81.34	77.36	92.91
Sim-Dot@800	82.83	77.36	92.54
Sim-Dot@900	83.83	78.10	92.17
Sim-Dot@1000	84.08	78.73	92.41
Sim-Dot@1500	85.32	80.34	93.78

Table 3: The effect of the size of \mathcal{D}_{aux} on detection performance with IMDB.

Method	5% noise	10% noise	20% noise
Sim-Cos@100	6.40	8.55	20.10
Sim-Cos@200	58.10	74.00	78.55
Sim-Cos@300	60.30	75.60	78.55
Sim-Cos@400	60.10	75.65	78.55
Sim-Cos@500	60.20	75.55	78.55
Sim-Cos@600	59.90	75.70	78.52
Sim-Cos@700	60.20	75.55	78.45
Sim-Cos@800	60.10	75.60	78.47
Sim-Cos@900	60.20	75.60	78.42
Sim-Cos@1000	59.90	75.50	78.52
Sim-Cos@1500	60.10	75.55	78.50
Sim-Dot@100	6.40	8.55	20.10
Sim-Dot@200	57.80	66.65	77.72
Sim-Dot@300	58.00	65.70	77.80
Sim-Dot@400	58.10	68.20	78.47
Sim-Dot@500	57.90	67.10	77.95
Sim-Dot@600	58.00	73.65	78.35
Sim-Dot@700	58.50	69.45	78.52
Sim-Dot@800	57.90	65.70	77.87
Sim-Dot@900	58.20	68.65	77.47
Sim-Dot@1000	59.90	68.60	77.55
Sim-Dot@1500	57.90	68.05	78.10

decrease after $k = 20$. This suggests that using larger k can harm the accuracy when the data is very noisy. For Sim-Dot with 10% and 20% noise in Tab. 4, the accuracy changes are less consistent across different values of k . This suggests that Sim-Dot may be more sensitive to the choice of k .

Table 4: Error detection accuracy of Sim-Cos and Sim-Dot changes as k changes with Snippets.

Method	5% noise	10% noise	20% noise
Sim-Cos@k=1	77.61	82.46	87.69
Sim-Cos@k=2	88.55	85.57	92.23
Sim-Cos@k=5	89.30	86.31	94.53
Sim-Cos@k=10	89.30	86.94	94.65
Sim-Cos@k=20	89.55	86.69	94.53
Sim-Cos@k=50	88.06	82.09	94.46
Sim-Cos@k=100	86.56	80.10	93.28
Sim-Cos@k=200	75.12	78.23	86.76
Sim-Dot@k=1	80.09	82.09	88.75
Sim-Dot@k=2	81.34	83.45	90.05
Sim-Dot@k=5	82.58	84.70	91.29
Sim-Dot@k=10	84.57	85.32	92.60
Sim-Dot@k=20	85.57	84.57	93.10
Sim-Dot@k=50	86.07	81.96	93.59
Sim-Dot@k=100	84.08	78.73	92.41
Sim-Dot@k=200	75.12	77.73	86.76

Table 5: The effect of k on detection performance with IMDB.

Method	5% noise	10% noise	20% noise
Sim-Cos@k=1	28.50	50.85	66.15
Sim-Cos@k=2	49.10	66.80	69.72
Sim-Cos@k=5	57.80	72.05	75.65
Sim-Cos@k=10	59.50	74.10	76.77
Sim-Cos@k=20	59.50	74.90	77.42
Sim-Cos@k=50	60.20	75.55	78.42
Sim-Cos@k=100	59.90	75.50	78.52
Sim-Cos@k=200	60.00	75.45	78.57
Sim-Dot@k=1	57.50	67.25	75.17
Sim-Dot@k=2	57.00	67.30	75.30
Sim-Dot@k=5	57.20	67.95	75.80
Sim-Dot@k=10	57.10	67.75	76.00
Sim-Dot@k=20	57.10	68.15	76.27
Sim-Dot@k=50	57.90	68.55	76.95
Sim-Dot@k=100	59.90	68.60	77.55
Sim-Dot@k=200	58.20	68.25	78.40

The effect of τ on error reduction rate. We analyze the effect of τ on the error reduction rate. We vary the number of $\tau = \{0.5, 0.6, 0.7, 0.8, 0.9, 0.99\}$. From results in Tab. 6 and Tab. 7, we see that for both Snippets and IMDB, the change of τ has minimal impact on the error reduction rate. Generally, the reduction rate is higher when the noise level is higher.

C.2 Correlation.

We calculate the Spearman correlation between ranking scores assigned to samples by detection methods. Fig. 3a shows that gradient-based, confident-based, and similarity-based methods have low Spearman correlation with each other. Confident-based and Gradient-based methods have

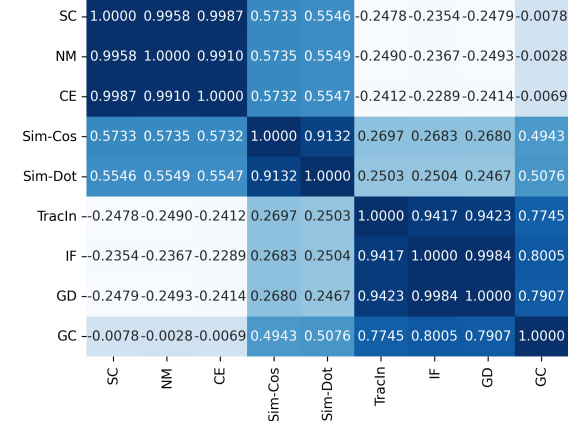
Table 6: Error Reduction Rate on Snippets.

Method	5% noise	10% noise	20% noise
Sim-Cos@ $\tau=0.5$	66.16	58.95	80.98
Sim-Cos@ $\tau=0.6$	50.74	58.83	77.00
Sim-Cos@ $\tau=0.7$	48.00	58.20	76.75
Sim-Cos@ $\tau=0.8$	46.51	57.83	76.69
Sim-Cos@ $\tau=0.9$	46.51	57.46	76.69
Sim-Cos@ $\tau=0.99$	46.51	57.46	76.69
Sim-Dot@ $\tau=0.5$	42.03	55.72	76.25
Sim-Dot@ $\tau=0.6$	43.03	56.34	76.38
Sim-Dot@ $\tau=0.7$	45.52	57.08	76.63
Sim-Dot@ $\tau=0.8$	46.26	57.33	76.69
Sim-Dot@ $\tau=0.9$	46.51	57.46	76.69
Sim-Dot@ $\tau=0.99$	46.51	57.46	76.69

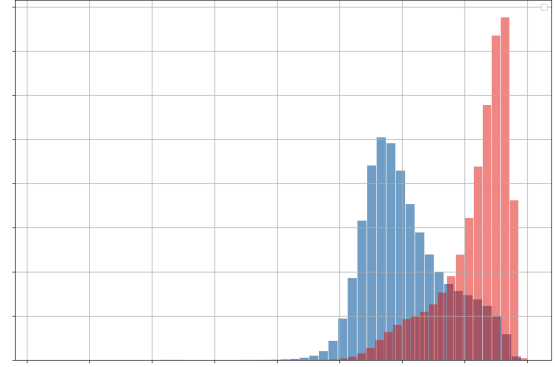
Table 7: Error Reduction Rate on IMDB.

Method	5% noise	10% noise	20% noise
Sim-Cos@ $\tau=0.5$	28.70	51.00	59.37
Sim-Cos@ $\tau=0.6$	28.40	41.15	59.12
Sim-Cos@ $\tau=0.7$	28.40	41.15	59.12
Sim-Cos@ $\tau=0.8$	28.40	41.15	59.12
Sim-Cos@ $\tau=0.9$	28.40	41.15	59.12
Sim-Cos@ $\tau=0.99$	28.40	41.15	59.12
Sim-Dot@ $\tau=0.5$	28.40	41.15	59.12
Sim-Dot@ $\tau=0.6$	28.40	41.15	59.12
Sim-Dot@ $\tau=0.7$	28.40	41.15	59.12
Sim-Dot@ $\tau=0.8$	28.40	41.15	59.12
Sim-Dot@ $\tau=0.9$	28.40	41.15	59.12
Sim-Dot@ $\tau=0.99$	28.40	41.15	59.12

negative Spearman correlation, indicating they are very different in ranking. We observed the same phenomenon in datasets across levels and types of noise.



(a) Spearman correlation of methods on Snippets with random noise 20%.



(b) Distribution of L_2 -norm ($\|\phi\|_2$) of features

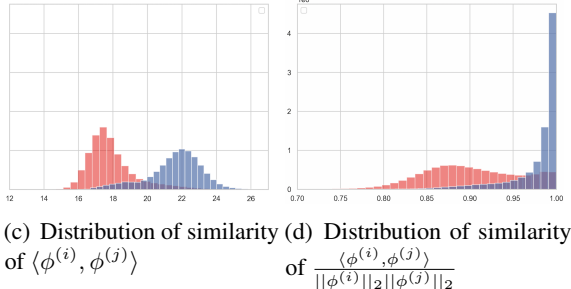


Figure 3: Visualization of (a) Spearman correlation, (b) the L_2 -norm of noisy data points (presented by blue bars) and normal data points (presented by red bars). Using normalization (Cosine; (d)) enables the differentiation of the similarity distribution, therefore, enhancing detection accuracy compared to the unnormalized approach (Dot; (c)).

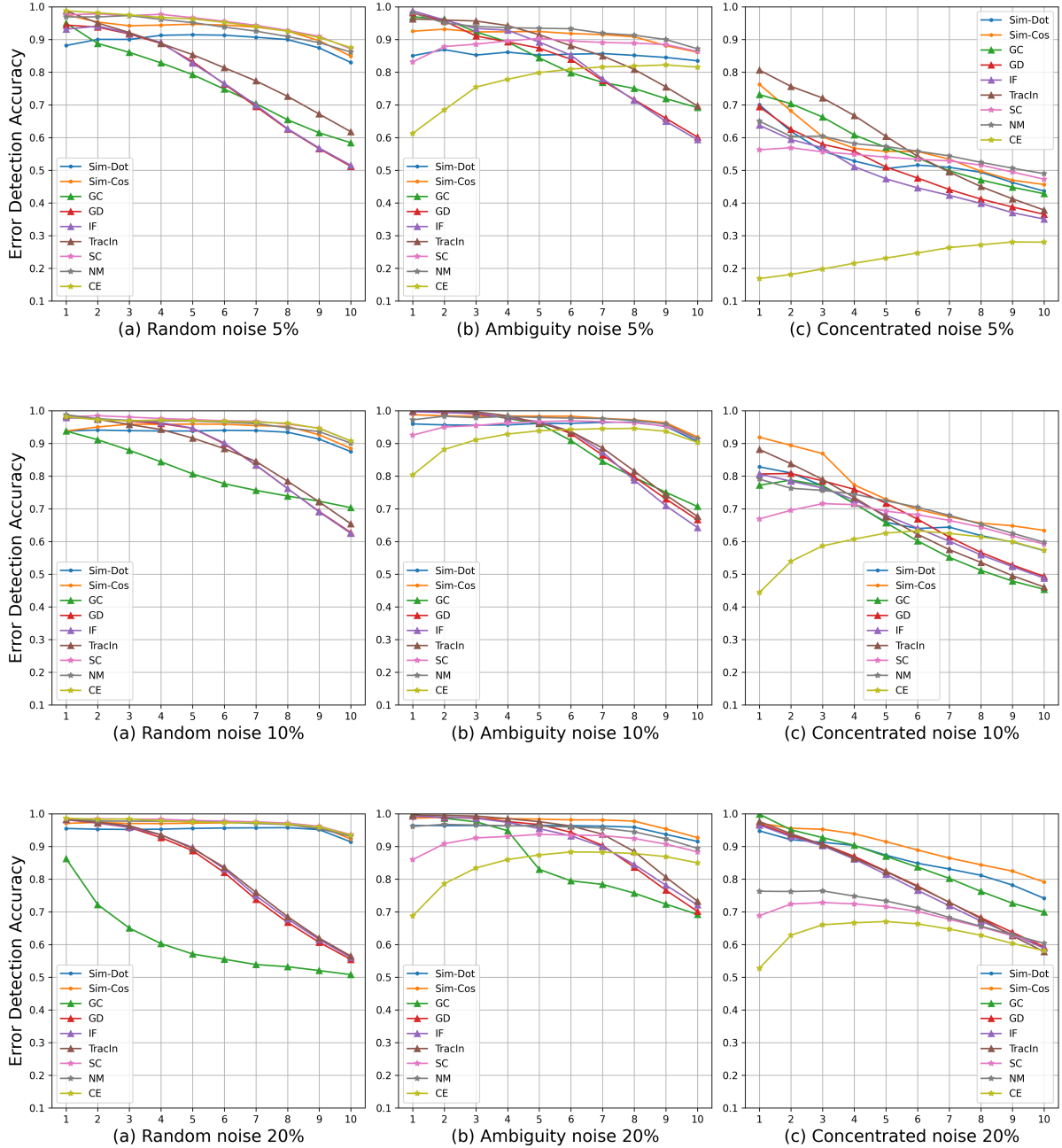


Figure 4: Detection accuracy of methods measured on Snippets with different levels of noise.

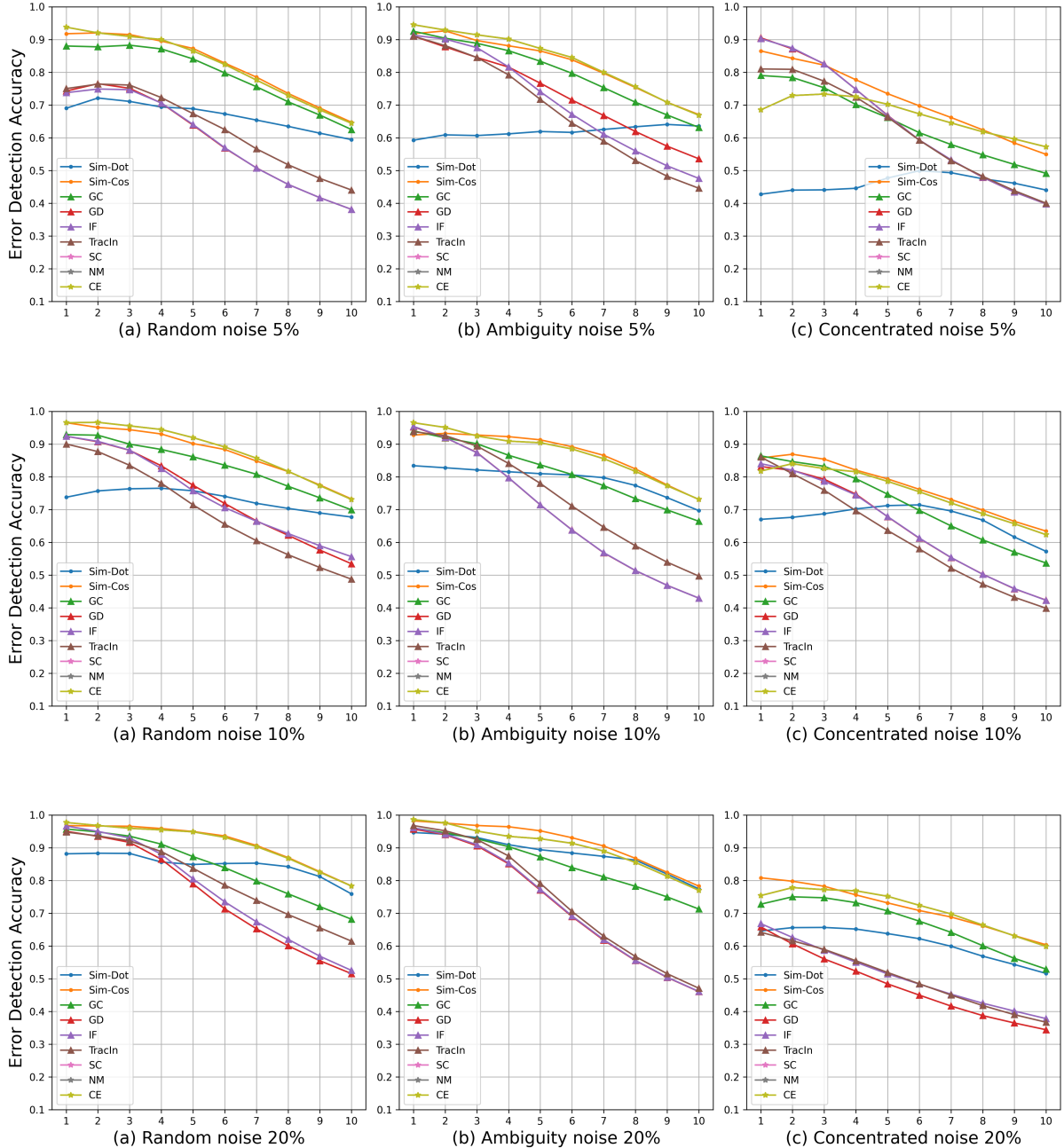


Figure 5: Detection accuracy of methods measured on IMDB with different levels of noise.

Table 8: Test accuracy on Snippets with 10% noise.

Method	Random noise		Ambiguity noise		Concentrated noise	
	Removed	Rectified	Removed	Rectified	Removed	Rectified
Acc. (under noise)	85.43 (+0.00)	—	88.24 (+0.00)	—	85.08 (+0.00)	—
Confidence-W. Entropy	88.07 (+2.64)	—	85.04 (-3.20)	—	84.56 (-0.52)	—
Normalize-Margin	81.75 (-3.68)	—	86.09 (-2.15)	—	79.73 (-5.35)	—
Self-Confidence	84.47 (-0.96)	—	87.06 (-1.18)	—	82.06 (-3.02)	—
Influence Function	90.04 (+4.61)	—	85.92 (-2.32)	—	81.36 (-3.72)	—
Gradient-Cosine	82.94 (-2.49)	—	81.18 (-7.06)	—	80.48 (-4.60)	—
Gradient-Dot	86.01 (+0.58)	—	85.13 (-3.11)	—	83.29 (-1.79)	—
TracIn	85.74 (+0.31)	—	86.88 (-1.36)	—	77.98 (-7.10)	—
Sim-Cos	79.73 (-5.70)	87.85 (+2.42)	85.48 (-2.76)	85.57 (-2.67)	81.58 (-3.23)	82.06 (-3.02)
Sim-Dot	88.29 (+2.86)	87.32 (+1.89)	84.34 (-3.90)	86.58 (-1.66)	81.62 (-3.46)	80.83 (-4.25)

Table 9: Test accuracy on Snippets with 5% noise.

Method	Random noise		Ambiguity noise		Concentrated noise	
	Removed	Rectified	Removed	Rectified	Removed	Rectified
Acc. (under noise)	87.14 (+0.00)	—	87.36 (+0.00)	—	87.93 (+0.00)	—
Confidence-W. Entropy	84.86 (-2.28)	—	86.57 (-0.79)	—	87.80 (-0.13)	—
Normalize-Margin	84.65 (-2.49)	—	84.82 (-2.54)	—	83.77 (-4.16)	—
Self-Confidence	85.35 (-1.79)	—	83.99 (-3.37)	—	86.09 (-1.84)	—
Influence Function	85.30 (-1.84)	—	86.00 (-1.36)	—	85.30 (-2.63)	—
Gradient-Cosine	85.43 (-1.71)	—	85.13 (-2.23)	—	79.51 (-8.42)	—
Gradient-Dot	84.56 (-2.58)	—	89.21 (+1.85)	—	87.06 (-0.87)	—
TracIn	84.65 (-2.49)	—	87.71 (+0.35)	—	81.88 (-6.05)	—
Sim-Cos	86.45 (-0.69)	85.17 (-1.97)	87.10 (-0.26)	85.48 (-1.88)	85.39 (-2.54)	87.19 (-0.74)
Sim-Dot	87.15 (+0.01)	87.06 (-0.08)	83.37 (-3.99)	84.34 (-3.02)	84.12 (-3.81)	79.82 (-8.11)

Table 10: Test accuracy on IMDB with 20% noise.

Method	Random noise		Ambiguity noise		Concentrated noise	
	Removed	Rectified	Removed	Rectified	Removed	Rectified
Acc. (under noise)	89.92	—	89.36	—	85.98	—
Confidence-W. Entropy	91.00 (+1.08)	—	90.73 (+1.37)	—	86.66 (+0.68)	—
Normalize-Margin	91.00 (+1.08)	—	90.73 (+1.37)	—	86.66 (+0.68)	—
Self-Confidence	91.00 (+1.08)	—	90.73 (+1.37)	—	86.66 (+0.68)	—
Influence Function	90.95 (+1.03)	—	90.51 (+1.15)	—	87.09 (+1.11)	—
Gradient-Cosine	90.59 (+0.67)	—	90.93 (+1.57)	—	86.78 (+0.80)	—
Gradient-Dot	90.43 (+0.51)	—	89.45 (+0.09)	—	82.87 (-3.20)	—
TracIn	90.19 (+0.27)	—	91.09 (+1.73)	—	82.87 (-3.20)	—
Sim-Cos	90.70 (+0.78)	88.73 (-1.19)	90.78 (+1.42)	90.83 (+1.47)	87.76 (+1.78)	84.73 (-1.25)
Sim-Dot	91.49 (+1.57)	90.46 (+0.54)	91.58 (+2.22)	90.13 (+0.77)	87.25 (+1.27)	87.46 (+1.48)

Table 11: Test accuracy on IMDB with 10% noise.

Method	Random noise		Ambiguity noise		Concentrated noise	
	Removed	Rectified	Removed	Rectified	Removed	Rectified
Acc. (under noise)	91.76 (+0.00)	—	91.68 (+0.00)	—	89.41 (+0.00)	—
Confidence-W. Entropy	91.79 (+0.03)	—	92.48 (+0.20)	—	90.95 (+1.54)	—
Normalize-Margin	91.79 (+0.03)	—	92.48 (+0.20)	—	90.95 (+1.54)	—
Self-Confidence	91.79 (+0.03)	—	92.48 (+0.20)	—	90.95 (+1.54)	—
Influence Function	91.65 (-0.11)	—	90.97 (-0.71)	—	86.26 (-3.15)	—
Gradient-Cosine	91.72 (-0.04)	—	91.29 (-0.39)	—	88.05 (-1.36)	—
Gradient-Dot	90.81 (-0.95)	—	92.10 (+0.42)	—	88.15 (-1.26)	—
TracIn	91.75 (-0.01)	—	91.66 (-0.02)	—	88.86 (-0.55)	—
Sim-Cos	91.12 (-0.64)	91.98 (+0.22)	92.52 (+0.84)	92.17 (+0.49)	90.15 (+0.74)	89.20 (-0.21)
Sim-Dot	91.38 (-0.38)	91.51 (-0.25)	91.52 (-0.16)	91.61 (-0.07)	89.78 (+0.37)	88.37 (-1.04)

Table 12: Test accuracy on IMDB with 5% noise.

Method	Random noise		Ambiguity noise		Concentrated noise	
	Removed	Rectified	Removed	Rectified	Removed	Rectified
Acc. (under noise)	91.67 (+0.00)	—	92.07 (+0.00)	—	91.52 (+0.00)	—
Confidence-W. Entropy	92.35 (+0.68)	—	92.58 (+0.51)	—	91.94 (+0.42)	—
Normalize-Margin	92.35 (+0.68)	—	92.58 (+0.51)	—	91.94 (+0.42)	—
Self-Confidence	92.35 (+0.68)	—	92.58 (+0.51)	—	91.94 (+0.42)	—
Influence Function	92.55 (+0.88)	—	91.76 (-0.31)	—	90.77 (-0.75)	—
Gradient-Cosine	92.46 (+0.79)	—	90.88 (-1.19)	—	89.78 (-1.74)	—
Gradient-Dot	91.79 (+0.12)	—	92.58 (+0.51)	—	90.32 (-1.20)	—
TracIn	92.62 (+0.95)	—	91.97 (-0.10)	—	91.45 (-0.07)	—
Sim-Cos	92.10 (+0.43)	92.10 (+0.43)	93.09 (+1.02)	92.50 (+0.43)	92.11 (+0.59)	91.74 (+0.22)
Sim-Dot	92.69 (+1.02)	92.06 (+0.39)	91.63 (-0.44)	91.09 (-0.98)	91.59 (+0.07)	90.96 (-0.56)